MICRO-CALORIMETERS WITH NTD AND EPITAXIAL GERMANIUM THERMISTORS FOR HIGH RESOLUTION X-RAY SPECTROSCOPY

NASA Grant No: NAG5-5269

REVISED

Progress Report No. 5

For Period 1 April 2004 through 31 March 2005

Principal Investigator
Dr. Eric Silver

May 2005

Prepared for:

National Aeronautics and Space Administration
Goddard Space Flight Center
Greenbelt, MD 20771

Smithsonian Institution
Astrophysical Observatory
Cambridge, Massachusetts 02138

> The Smithsonian Astrophysical Observatory
> is a member of the
> Harvard-Smithsonian Center for Astrophysics

The NASA Technical Officer for this Grant is John Brinton, Code 810, Wallops Flight Facility; Wallops island, VA 23337

1. Introduction

This is a progress report for the third year of a three year SR&T grant to continue the advancement of NTD-based microcalorimeters. We highlight our progress to date that allowed us to garner an additional three years of funding for this work.

1.1 Energy Resolution and Dynamic Range

Thermistor Response: We have made significant advances in understanding our single pixel NTD-Ge based microcalorimeters and electronics system. With high count rate spectroscopy as a goal, we introduced in 1989 a new approach to low noise pulse counting electronics for microcalorimeters (Silver et al., 1989). The circuit configuration shown in Figure 1.1 is based upon the specific design of a JFET preamplifier that Goulding, Landis and Pehl (1969) developed for use with silicon and germanium charge collecting detectors. Previous designs for calorimeter preamplifiers (Moseley et al. 1984) bias the thermistor with a constant current and use a source follower read-out circuit where the combination of the calorimeter resistance and the input
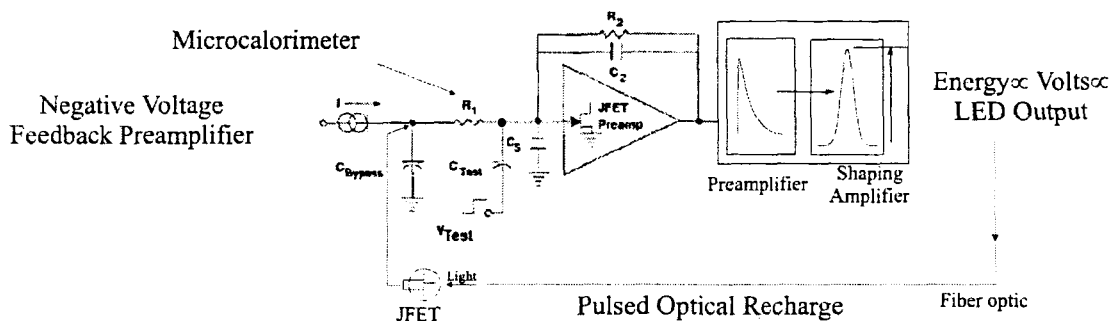

Figure 1.1 The negative voltage feedback preamplifier with pulse optical recharge circuit.

capacitance determine the temporal response. The response time (thermal rise time) in the source follower is typically limited to 100-200μs and is a property of the electronic circuit. Our design employs negative voltage feedback which significantly improves the capability of measuring signal rise times of the calorimeter. The virtual ground established at the input to the JFET allows the preamplifier to track transient signals with risetimes that are as short as the time constant of the feedback element (<20μs). This is shorter than the thermalization time of the detector. Consequently, this circuitry has made it possible to build NTD microcalorimeters with thermal recovery times that are less than 200 μs.

The negative voltage feedback amplifier allows the calorimeter to be operated with either

a constant voltage across the thermistor or a constant current through it. In the constant current mode, a voltage, $V \propto I_{const} \times R$, is measured at the preamplifier input while in the constant voltage mode, a current, $I \propto V_{const} / R$, is measured by the preamplifier. The fact that the resistance value decreases when a signal occurs results in positive thermal feedback in the V_{const} mode because the V^2/R self-heating power adds to the signal heating. Negative feedback occurs in the I_{const} mode. Indeed, under certain conditions, thermal runaway could occur in the V_{const} mode. We have demonstrated experimentally that we can operate our microcalorimeters with excellent performance without approaching the thermal runaway limit. These biasing configurations each have their advantages but those of the constant voltage mode outweigh those of the constant current case for high count rate and broad bandwidth applications. As shown below, it provides greater responsivity, or higher effective alpha, and is intrinsically more linear, especially at high energies and thereby provides better energy resolution and much larger dynamic range compared to the constant current configuration.
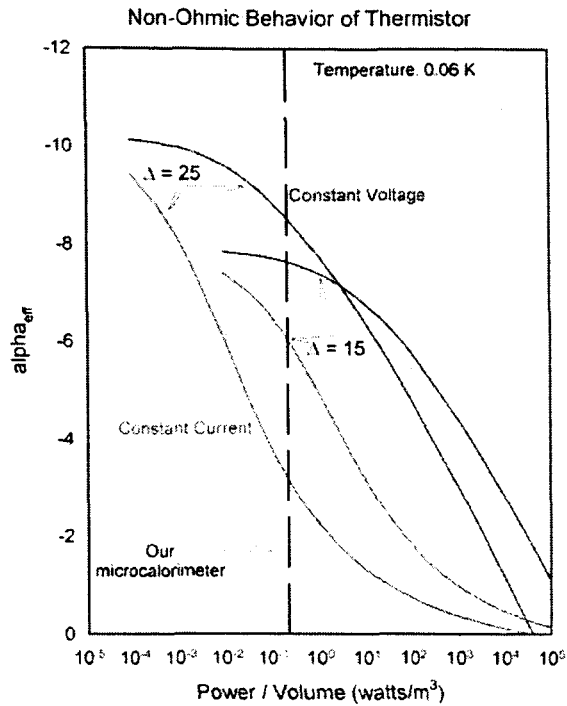
Non-Ohmic Behavior of Thermistor

Figure 1.2 $\alpha_{effective}$ of a thermistor as a function of bias power density for I_{const} and V_{const}

Careful characterization of thermistors has shown that the thermistor resistance decreases with increasing bias power. This non-ohmic effect is substantially larger than expected purely from the reduction in resistance due to joule heating. The behavior occurs in ion-implanted silicon and NTD-Ge and has been characterized over a wide range of doping densities (Zhang et al.,1998) using empirical models. It has a greater detrimental impact on the I_{const} mode than on the V_{const} configuration. Figure 1.2 shows a comparison at 60 mK of the effective responsivity, $\alpha_{effective}$ vs. power density for two different doping concentrations denoted by Δ. $\alpha_{effective}$ includes the non-ohmic behavior of the thermistor . The curves show that the responsivity for a thermistor biased with a constant voltage is significantly greater over a larger range of power densities than for a thermistor in constant current mode. $\alpha_{effective}$ for constant current operation drops significantly at a power density that is at least an order of magnitude lower than for the same thermistor biased with constant voltage.

Since a typical NTD thermistor volume is at least 100 times that of ion-implanted silicon, NTD thermistors can operate with higher power and maintain the same value of $\alpha_{effective}$. (The reader is reminded that the total heat capacity of the NTD microcalorimeters is comparable to that of ion-implanted devices, but the distribution between components differs). This also means that NTD microcalorimeters can have higher detection speed. The quiescent thermal operating point of the detector above the temperature of the
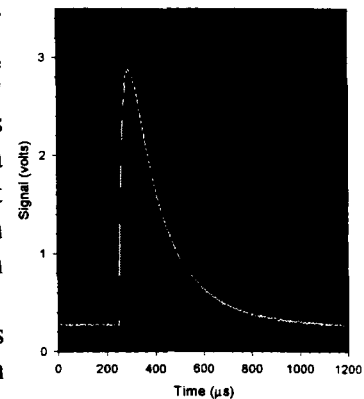

Figure 1.3. Typical temporal profile from a 6 keV x-ray.

cold stage is determined by the bias power and the thermal conductance, G. Since an increase in G makes the detector faster, the bias power must be increased to maintain the optimal quiescent temperature of the detector. In turn, the volume must be increased to maintain the power density and sensitivity. Since NTD thermistors can be made relatively large ($\sim 10^{-13}$ m^3) without greatly influencing the heat capacity, we operate them with relatively high power compared to ion-implanted silicon thermistors. G can therefore be made larger, thereby increasing the detector speed, as evidenced by the temporal profile shown in Figure 1.3.

Static and Dynamic Noise: However, this does not tell the entire story. The question is whether the positive electrothermal feedback introduced by constant voltage bias has an effect on the detector noise that counteracts the advantages described above? Since the thermistor resistance and its temperature both vary during an x-ray event, the dynamic changes in the component noise sources, (i.e., Johnson, JFET, phonon and 1/f) must be taken into account in all noise calculations. We define the noise during the x-ray pulse as *dynamic* noise and distinguish it from the *static* noise which is characteristic of the microcalorimeter in the absence of x-rays. This problem was appreciated previously by workers in the field but analysis of noise, traditionally performed in the frequency domain, does not permit a good assessment of the noise. Goulding (2002) has developed an integrated, time-domain approach to the analysis of noise performance that handles the behavior of time-variant circuit elements. We have used this technique to simulate the performance of our microcalorimeters, including the time-dependence of resistance and temperature during the x-ray-induced event.

In the I_{const} mode, the mean square voltage noise per unit frequency is $4kTR$, and in the V_{const} mode the equivalent mean square current noise is $4kT / R$. During an x-ray event, the temperature rises and the value of the thermistor resistance decreases by a larger factor than that of the temperature. In the V_{const} mode, the two effects are additive so the Johnson noise clearly increases in the presence of a signal. In the I_{const} mode the temperature rise tends to increase the noise but this is more than offset by the reduction in the resistance, so the Johnson noise decreases in the presence of a signal. While the general behavior is intuitively obvious, a quantitative estimate of the final result can only be obtained by integrations in a piecewise manner, since the temperature and
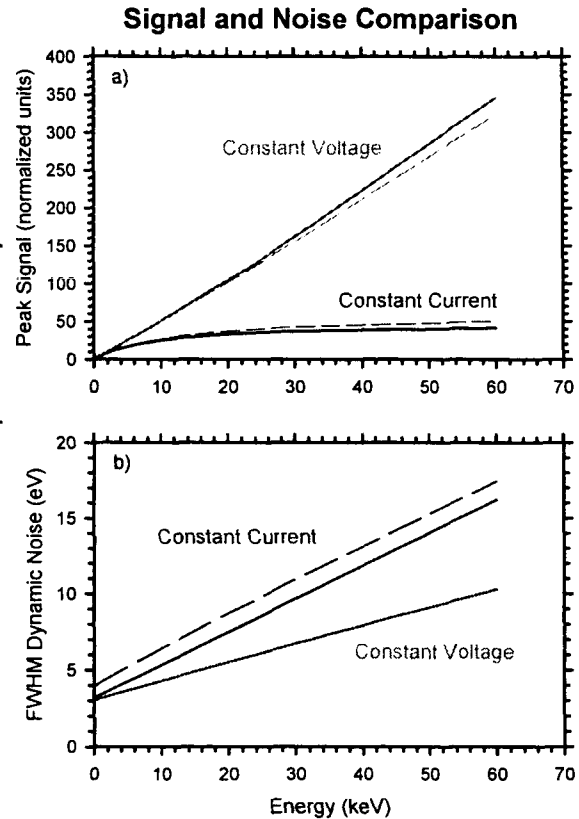

Signal and Noise Comparison

Figure 1.4 a) The variation of the peak signal vs x-ray energy for the V_{const} (red)and I_{const}(blue) modes. The dashed curves include the non-ohmic thermistor behavior. b) The predicted energy resolution (total dynamic noise) for both modes. The dashed blue curve for I_{const} includes the non-ohmic behavior. The difference between the dashed and solid curves for V_{const} is less than the line thickness on the plot. Parameters:Bias=300pA;R_{init}=1x10^{7}Ω;Δ=15K;Base temp=0.06K;equil temp=0.062K;heat capacity=1x 10$^-$ ^{13}J/K;τ_{nse}=65µs;τ_{decay}=500µs;sin^4 shaper peaking at 400µs.

resistance values have a steady state value prior to the arrival of the x-ray followed by a time-variable value determined by the signal characteristics.

Signal to Noise: Our simulation takes all these effects into account for all noise components and we present an example for *nominal* detector parameters. Figure 1.4a shows the variation in the output signal peak amplitude with energy (the amplitudes are normalized to the value at 200 eV to enable the comparison between the two modes of bias; the dashed curves include the non-ohmic behavior of the thermistor) . We see that the two modes differ drastically in their linearity. The I_{const} mode exhibits severe non-linearity at higher energies due to the voltage across R approaching its limit (I_{bias} x R_{init}; R_{init} is

Figure 1.5 The JFET noise for 3 values of drain current.

the resistance value of the thermistor before the x-ray event). In Figure 1.4b the FWHM dynamic noise (i.e., total energy resolution) in the signal peak is plotted. Note that the non-linearity in the signal in the I_{const} mode causes severe degradation in the energy resolution particularly at high energies. This is perhaps surprising but it results from the fact that the baseline fluctuations at the time the signal reaches its peak are determined by the earlier noise impulses filtered and stored in the filter network. This fluctuation is in no way affected by the non-linearity (Goulding, 2002). It is evident from these calculations that for the same microcalorimeter, the V_{const} mode offers better resolution performance, particularly at high energies.

In our work leading up to our previous proposal, we identified an aspect of the feedback circuit that could introduce spectral broadening if modifications were not made. When the calorimeter absorbs a photon, the thermistor resistance drops and the stored charge on the capacitor, C_{bypass}, (see Figure 1.1) provides the appropriate current needed to maintain a constant voltage across the calorimeter. This additional current passes through the feedback resistor to produce the output signal. Following an x-ray event, this capacitor recharges by diverting bias current from the thermistor which then cools below its original quiescent value until the capacitor is fully recharged. This effect causes spectral smearing as the photon rate increases.
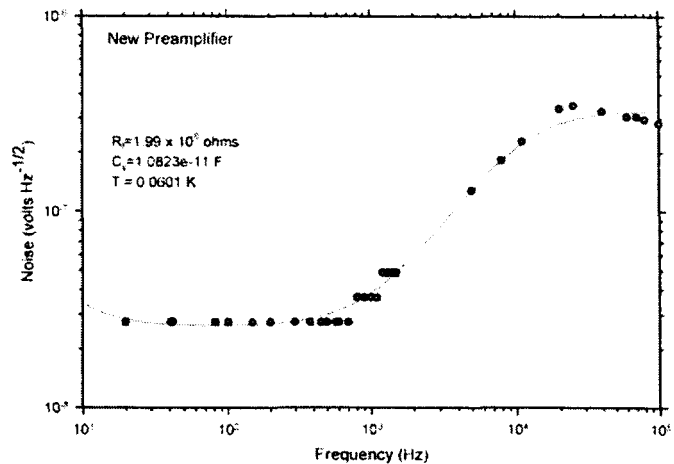

Figure 1.6 The combined noise of the JFET and feedback resistor; blue dots are the measured values and the black curve is the theoretical fit. The detector's thermistor is not included in these measurements

To remedy this situation, we developed an electro-optical circuit that restores the charge

extracted from the bypass capacitor. A very small commandable current was created by coupling a light emitting diode(LED) through a fiber optic cable onto the reversed biased gate-source junction of an extremely low leakage junction field effect transistor (JFET). The low leakage JFET is connected in parallel with the output of the constant current source. A drive signal for the LED is derived by examining the proportional signal out of the pulse processing (shaping) amplifier in real time.

Using this prototype electro-optical circuit we achieved an energy resolution of 4.8 eV at 6 keV using analog pulse processing. This microcalorimeter had a tin (Sn) x-ray absorber(0.4 mm x 0.4 mm x 7 μm) and a thermistor of NTD germanium (250 μm x 50 μm x 50 μm.) The quantum efficiency of this detector is 95% at 6 keV. (Silver et al. 2002)

1.4 Recent work

More recently, we have made several significant advances that have led to a reduction in low frequency (1/f) noise, improved stability, and resolution performance of 3.08 eV at 6 keV. This is now consistent with our theoretical model which also predicts sub 2 eV at 1 keV.

Noise Measurements and JFET Preamplifier Stability: High open loop gain is essential for the operation of our negative feedback , virtual ground preamplifier. It has intrinsically higher bandwidth and lower absolute noise than the source follower topology, but it requires substantial transconductance or gain, g_m, from the JFET. g_m is a strong function of the applied drain current ($g_m \propto I_d^{1/2}$) while the JFET noise, to first order, is proportional to $1/g_m^{1/2}$ (typically 0.5 - 1.5 nV/Hz$^{1/2}$).

We suspected that the noise from the JFET was excessive at low frequencies and carefully evaluated the noise contributions from the feedback resistor and the JFET. A special, AC grounded gate, preamplifier was built to measure the noise of the in-situ JFET independent of the feedback resistor. Figure 2.5 is a plot of JFET noise vs frequency for a JFET operated with several different amounts of drain current. We learned that by reducing the drain current below 1 mA, we were able to significantly reduce the low frequency noise (1/f noise) while incurring only a modest rise in the higher frequency noise.
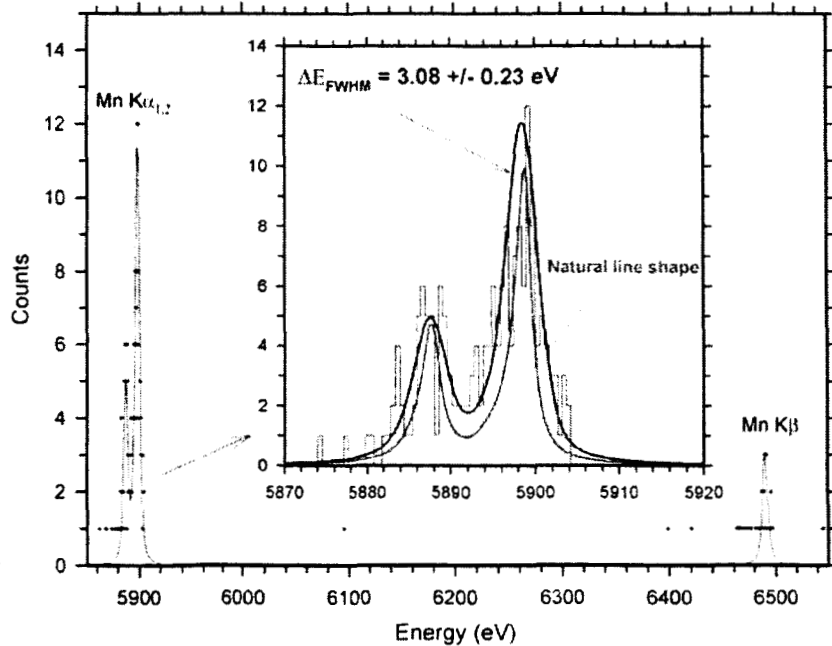
However, the transconductance of the

Figure 1.7 Our most recent microcalorimeter measurement of the K lines of an [55]Fe radioactive source. The expanded view shows the Kα$_1$ and Kα$_2$ line shapes in red and the microcalorimeter's measurement in blue.

JFET, already modest at higher currents, dropped a further factor of two when the drain current was reduced to the lower levels needed at the desired low frequency, low noise operating point. The open loop gain of the preamplifier (originally ~ 2000) was also reduced a further factor of two. This reduction in open loop gain caused us to reconsider the issue of virtual ground stability and dynamic impedance. Our solution, an entirely new preamplifier topology, overcomes the limitations of our previous preamplifier. The new preamplifier has an open loop gain > 100,000 when the JFET is operated at a reduced drain current and provides low noise at low frequencies. With this large open loop gain, the issues of virtual ground dynamic impedance and stability are gone. Serendipitously, the new preamplifier topology also requires less power and has fewer components.

An additional set of measurements were performed to verify that the combined noise from the JFET and feedback resistor was what one expected from theoretical predictions. In Figure 1.6, data is plotted in blue and a theoretical fit (black curve) based upon the measured feedback resistance and capacitance values, circuit stray capacitance and independent JFET noise measurements (from Figure 1.5). Not only do these results show that the circuitry is now well understood, but the preamplifier circuitry produced immediate improvements in the performance of our NTD germanium microcalorimeters.

In Figure 1.7 we plot the spectrum of the Mn $K\alpha$ and $K\beta$ lines from an ^{55}Fe radioactive source. The expanded view shows $K\alpha_1$ and $K\alpha_2$ natural line shapes in red and the microcalorimeter's measurement in blue. The microcalorimeter resolution is 3.08 ± 0.23 eV (Silver et al. 2005).

Theoretical Calculations: As mentioned above, we have developed a theoretical model to predict the performance of our NTD microcalorimeters. In Figure 2.8a below, we plot the contributions to the total noise in units of eV as a function of energy for the microcalorimeter used to measure the spectrum in Figure 1.7. The characteristics of the microcalorimeter are listed at the top left of the figure. The largest contribution to the noise below 10 keV comes from the thermistor followed by the phonon noise and JFET noise. We remind the reader that the *dynamic* resolution increases with
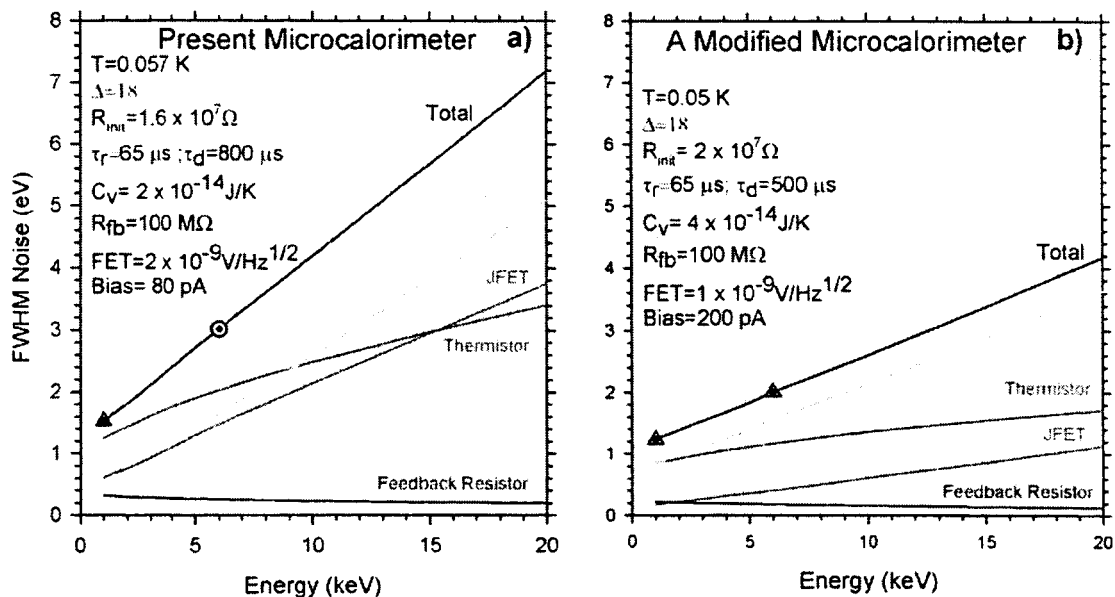

Figure 1.8 The model predictions for the total dynamic noise (energy resolution) and the contributing noise components a) for the detector that produced the spectrum in Figure 2.7; b) the predictions for a modest change in the detector's properties and operating conditions.

energy because in the constant voltage mode, the thermistor noise current goes as $1/R^{1/2}$ and the JFET noise expressed as an input current goes as $1/R$. Since the thermistor resistance decreases as the microcalorimeter absorbs the energy of an x-ray, these noise components will increase. The phonon noise also increases because it reflects the microcalorimeter temperature during an x-ray event. (See discussion leading to Figure 2.4). (The feedback resistor does not have a dynamic noise component.) This model describes the performance of our microcalorimeter at 6 keV (⊙ in Figure 1.8a) quite well and also predicts that the resolution should be 1.7 eV at 1 keV (Δ in Figure 1.8a). Our

Figure 2.1. The spectrum of emissions from [241] Am and [55] Fe sources. The Np L lines between 13.7 keV and 20.8 keV produced in the [241] Am decay have been absorbed by a copper foil.

measurements at 1 keV are larger and we recognize now that there may be a noise floor set either by the components of the active current source or by noise sources following the preamplifier that we have not studied carefully enough. We will investigate the source of this noise during the next year. In Figure 1.8b we predict the performance for a modest change in detector parameters. We believe that with a slight decrease in JFET noise and a modest increase in thermistor resistance and current bias, a resolution of 2 eV at 6 keV can be achieved.

2.0 Hard X-ray Performance

We have extended the bandpass of the NTD-Ge microcalorimeter into the hard x-ray range by increasing the thickness of the absorber. Figure 2.1 shows the spectrum of [55]Fe and [241]Am obtained with a detector operating at a base temperature of 80 mK and dimensions of 0.5 mm x 0.5 mm x 25 μm. The quantum efficiency (Q.E.) is 40% at 35 keV and 8% at 68 keV. The broad band, high resolution response of the microcalorimeter is evident and the figure includes expanded views of the 60 keV line from [241]Am and the 5.89 keV and 6.4 keV lines emitted when the [55]Fe decays to manganese. (The low energy
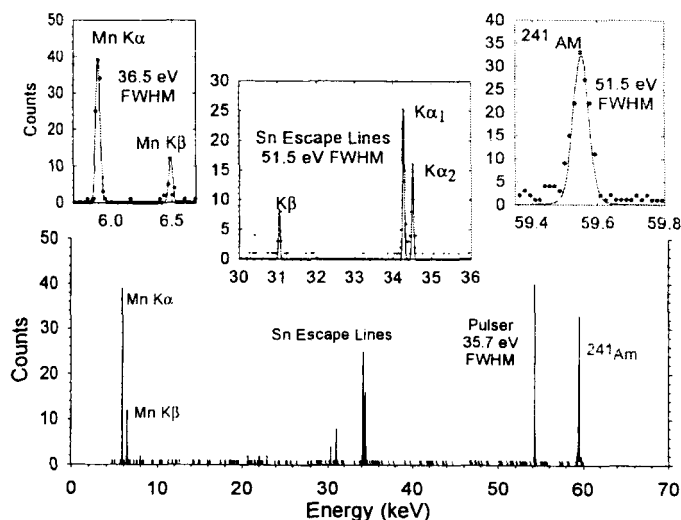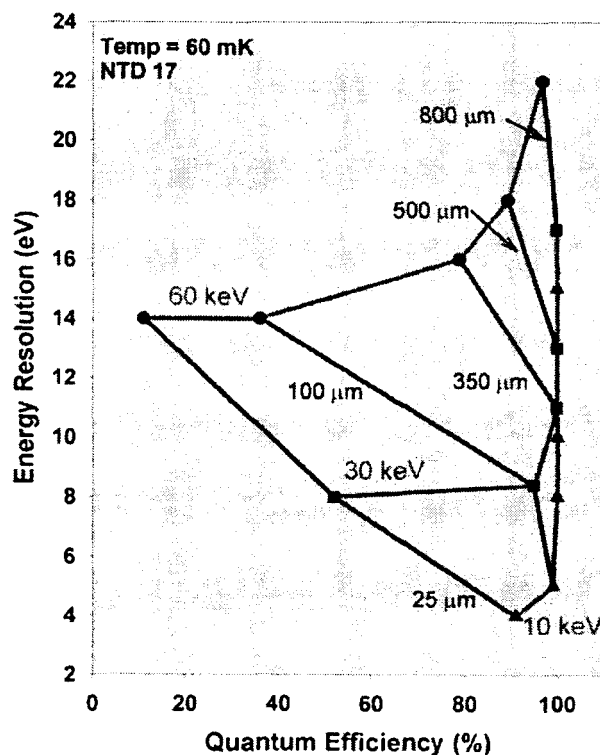

Figure 2.2. Predictions of energy resolution as a function of tin absorber quantum efficiency for three x-ray energies, 10 keV, 30 keV and 60 keV and 5 absorber thicknesses. The operating temperature is 60 mK

neptunium L lines between 13.7 keV and 20.8 keV that are produced in the [241]Am decay have been suppressed by a copper foil.) The spectrum also includes a contribution from the $K\alpha_1$, $K\alpha_2$ and K β escape peaks from the tin absorber. These $K\alpha$ and K β lines appear ~25 keV and ~28 keV, respectively, below the 60 keV line and are easily resolvable. The energy resolution at 35 keV and 60 keV is 51 eV, while at 6 keV it is 36 eV.

The implications of our recent this technical advancements at low energies offer tantalizing possibilities for the performance in the 10 keV to 70 keV range as well. Our detector modeling codes have confirmed that the 50 eV energy resolution at 60 keV for our early detectors (figure 2.1) was dominated by front-end preamplifier noise. The resolution should have been 30 eV for the type of microcalorimeter components used at that time. The earlier microcalorimeter also was intrinsically less sensitive than the one used for the recent soft x-ray measurements. Thus, we can expect further improvement by adapting this more sensitive detector to this high energy application. (Silver et al. 2004)

In Figure 2.2 we show the relationship between energy resolution and absorber quantum efficiency for three x-ray energies, 10 keV, 30 keV and 60 keV as determined from our computer model. By incorporating our recent detector advancements, we can choose to use a 350 μm thick tin absorber to achieve 80% quantum efficiency at 60 keV while maintaining an energy resolution of 14 eV. We will evaluate these ideas during the next research period.

References
Goulding, et al., 1969, in *Semiconductor Nuclear-Particle Detectors and Circuits*, ed. W. Brown, W. Higinbotham, G. Miller, and R. Chase, Washington, DC, National Academy of Sciences, 455,169.
Goulding, F. , 2002, *Nuclear Instruments and Methods in Physics Research* **A 485**, 653.
Silver, E., et al. , 1989 , *Proc. SPIE* **1159**, 423.
Silver, E., et al., 2000, *Nuclear Instruments and Methods in Physics Research* **A 444**, 156.
Silver at al., 2005, to appear in the Proceedings of *X-ray Diagnostics for Astrophysical Plasmas: Theory, Experiment, and Observation*, 2004, November 15-17,Cambridge, Massachusetts, USA
Zhang et al., 1998, *Phys. Rev. B.*, **57**,4472.

Talks and Papers Presented During this Reporting Period

High Energy, High Resolution X-Ray Spectroscopy:Microcalorimeters For Nuclear Line Astrophysics ,E. Silver, H. W. Schnopper, C. Jones, W. Forman, S. Romaine, N. Madden, D. Landis, J. Beeman, E. E. Haller, M. Barbera, F. Christensen, B. Ramsey, S. Woosley and R. Diehl, invited talk presented at the *Workshop on X-ray Diagnostics for Astrophysical Plasmas: Theory, Experiment, and Observation*, 2004, November 15-17,Cambridge, Massachusetts, USA.

A NTD Germanium-Based Microcalorimeter With 3.1 eV Energy Resolution At 6 keV, E. Silver, G.Austin, J. Beeman, F. Goulding, E.E. Haller, D. Landis and N. Madden, to be appear in *Nuclear Instruments and Methods in Physics Research* A , 2005.